Yu-Shiba-Rusinov states of impurities in a triangular lattice of $NbSe_2$ with spin-orbit coupling

Andrzej Ptok,[1,2,*] Szczepan Głodzik,[2,†] and Tadeusz Domański[2,‡]

[1]*Institute of Nuclear Physics, Polish Academy of Sciences, ul. E. Radzikowskiego 152, 31-342 Kraków, Poland*

[2]*Institute of Physics, Marie Curie-Skłodowska University, pl. Marii Skłodowskiej-Curie 1, PL-20031 Lublin, Poland*

(Received 5 July 2017; revised manuscript received 31 October 2017; published 22 November 2017)

We study the topography of the spin-polarized bound states of magnetic impurities embedded in a triangular lattice of a superconducting host. Such states have been observed experimentally in 2H-$NbSe_2$ crystal [G. C. Ménard *et al.*, Nat. Phys. **11**, 1013 (2015)], and they revealed oscillating particle-hole asymmetry extending to tens of nanometers. Using the Bogoliubov–de Gennes approach, we explore the Yu-Shiba-Rusinov states in the presence of spin-orbit interaction. We also study the bound states of double impurities for several relative positions in a triangular lattice.

DOI: 10.1103/PhysRevB.96.184425

I. INTRODUCTION

Magnetic impurities are detrimental for Cooper pairs because they induce spin-polarized subgap states [1–3] and (when impurities are dense enough) partly suppress or completely fill in the energy gap of the superconducting sample. Such in-gap quasiparticles, dubbed Yu-Shiba-Rusinov (YSR) states [4–6], have been observed experimentally in various systems [7–14]. They always exist in pairs, appearing symmetrically with respect to the chemical potential (treated here as the "zero-energy" reference level). Their energies can be controlled either electrostatically or magnetically [14]. Another feature is their spin-polarization evidenced by the asymmetric conductance at opposite voltages [15,16].

The bound states formed at magnetic impurities in three-dimensional isotropic superconductors are usually characterized by a relatively short spatial extent [17]. Contrary to that, in two-dimensional (2D) lattices, Ménard *et al.* [11] have reported different behavior, displaying a much longer extent of the YSR states with alternating (oscillating) particle-hole spectral weights. Furthermore, the bound states of impurities in superconducting 2H-$NbSe_2$ [18] with *quasi*-2D triangular lattice structure and strong spin-orbit coupling [19] have revealed the long-range coherent structures of a star-shape, whereas molecular dimers developed more complex spatial features [20].

Bulk crystals of 2H-$NbSe_2$ are characterized by centrosymmetric ($P6_3/mmc$) structure, formed by the stacking of noncentrosymmetric layers [21,22] [Fig. 1(a)]. Every layer is arranged in a honeycomb structure, comprising Nb and Se sublattices. Local inversion symmetry breaking [23–25] gives rise to the out-of-plane spin polarization [21] in every layer. At $T_{CDW} \approx 33$ K, there appears charge-density order [22,26,27], and below $T_c \approx 7$ K [21] the superconducting state sets in.

The normal state Fermi surface, studied by angle-resolved photoemission spectroscopy (ARPES) [21,27–30], has revealed two pairs of Nb-derived pockets, which are trigonally warped around a central Γ point and at the corner of the (hexagonal) first Brillouin zone. *Ab initio* (DFT) calculations indicated that the Fermi surface sheets originate predominantly from Nb 4*d* orbitals [21,31–33]. As a consequence, a triangular lattice formed by Nb atoms plays an important role for the superconducting state of this compound [34] and implies further a unique starlike shape of the bound states.

Contrary to bulk systems, the Fermi surface of the single monolayer 2H-$NbSe_2$ consists of only the pockets around the corner points of the Brillouin zone [21], whose size depends on the spin polarization [Fig. 1(b)]. The latter effect originates from the in-plane spin-orbit field [19,30]. Coupling of the spin to the *valley* distinguishes between nonequivalent parts of the Brillouin zone. Similar behavior has also been observed in other materials with hexagonal lattice structures [36–39].

Motivated by the recent experimental results of Ménard *et al.* [11], we study the YSR states of magnetic impurities embedded in a triangular lattice of the 2D superconducting host. The single monolayer of the 2H-$NbSe_2$ can be treated as a two-dimensional triangular lattice [34] with an in-plane spin-orbit field (in the supplemental material, we take into account also the out-of-plane spin-orbit component, which might be realized in other compounds [40,41]).

In Sec. II we present the microscopic model and discuss some methodological details. Next, in Sec. III A, we analyze the YSR bound states of a single magnetic impurity in a

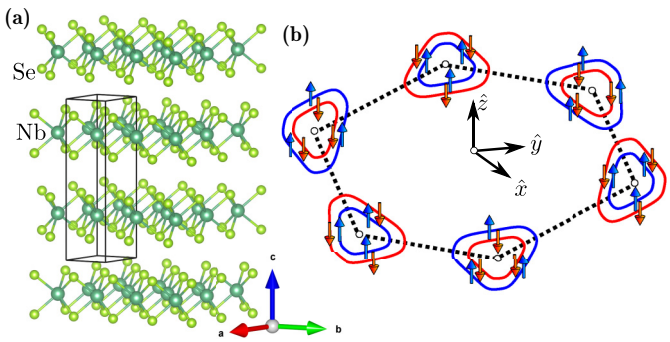

FIG. 1. (a) Crystallographic structure of the centrosymmetric $NbSe_2$ compound and its primitive unit cell (black prism). The image was obtained using VESTA software [35]. (b) Schematic view of the Fermi surface in the $NbSe_2$ monolayer, adopted from Ref. [21]. Blue (red) corresponds to different spin [negative (positive)] polarizations for each Fermi sheet in the zone corners.

*aptok@mmj.pl
†szglodzik@kft.umcs.lublin.pl
‡doman@kft.umcs.lublin.pl

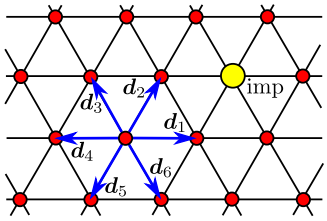

FIG. 2. Schematic illustration of a single magnetic impurity (yellow) in a two-dimensional triangular lattice. Each lattice site is surrounded by six nearest neighbors at positions $\boldsymbol{d}_\alpha$.

triangular lattice (Fig. 2), focusing on the role of spin-orbit coupling. In Sec. III B we study the bound states of double magnetic impurities (arranged in three different configurations) that might be relevant to the experimental data [20] revealing strong interference effects. Finally, in Sec. IV we summarize the main results.

II. MODEL AND METHOD

Magnetic impurities embedded in a 2D superconducting host with spin-orbit coupling can be described by the following Hamiltonian:

$$\hat{\mathcal{H}} = \hat{\mathcal{H}}_0 + \hat{\mathcal{H}}_{\rm imp} + \hat{\mathcal{H}}_{\rm int} + \hat{\mathcal{H}}_{\rm SOC}. \tag{1}$$

The single-particle term

$$\hat{\mathcal{H}}_0 = -t \sum_{\langle i,j\rangle\sigma} \hat{c}^\dagger_{i\sigma}\hat{c}_{j\sigma} - \mu \sum_{i\sigma} \hat{c}^\dagger_{i\sigma}\hat{c}_{i\sigma} \tag{2}$$

describes the kinetic energy of electrons, where $\hat{c}^\dagger_{i\sigma}$ ($\hat{c}_{i\sigma}$) denotes the creation (annihilation) of an electron with spin σ at the ith lattice site, t is a hopping integral between the nearest neighbors, and μ is the chemical potential. Large spin S of the impurities can be treated classically [1,2], and in such a case the interaction potential can comprise the magnetic J and nonmagnetic K parts,

$$\hat{\mathcal{H}}_{\rm imp} = -J(\hat{c}^\dagger_{0\uparrow}\hat{c}_{0\uparrow} - \hat{c}^\dagger_{0\downarrow}\hat{c}_{0\downarrow}) + K(\hat{c}^\dagger_{0\uparrow}\hat{c}_{0\uparrow} + \hat{c}^\dagger_{0\downarrow}\hat{c}_{0\downarrow}). \tag{3}$$

We describe the superconducting state, imposing the on-site interaction

$$\hat{\mathcal{H}}_{\rm int} = U \sum_i \hat{c}^\dagger_{i\uparrow}\hat{c}_{i\uparrow}\hat{c}^\dagger_{i\downarrow}\hat{c}_{i\downarrow} \tag{4}$$

with attractive potential $U < 0$. Such effective pairing is assumed to be weak, therefore we can treat it within the standard mean-field decoupling

$$\begin{aligned}\hat{c}^\dagger_{i\uparrow}\hat{c}_{i\uparrow}\hat{c}^\dagger_{i\downarrow}\hat{c}_{i\downarrow} = {}& \chi_i \hat{c}^\dagger_{i\uparrow}\hat{c}^\dagger_{i\downarrow} + \chi_i^* \hat{c}_{i\downarrow}\hat{c}_{i\uparrow} - |\chi_i|^2 \\ & + n_{i\uparrow}\hat{c}^\dagger_{i\downarrow}\hat{c}_{i\downarrow} + n_{i\downarrow}\hat{c}^\dagger_{i\uparrow}\hat{c}_{i\uparrow} - n_{i\uparrow}n_{i\downarrow},\end{aligned} \tag{5}$$

where $\chi_i = \langle \hat{c}_{i\downarrow}\hat{c}_{i\uparrow}\rangle$ is the superconducting order parameter and $n_{i\sigma} = \langle \hat{c}^\dagger_{i\sigma}\hat{c}_{i\sigma}\rangle$ is the average number of spin σ particles at the ith site. The Hartree term can be incorporated into the *effective* local spin-dependent chemical potential $\mu \to \tilde{\mu}_{i\sigma} \equiv \mu - U n_{i\bar{\sigma}}$. As we shall see, impurities suppress the local order parameter χ_i whose magnitude and sign depend on the coupling strength J [42,43].

The spin-orbit coupling (SOC) can be expressed by [44]

$$\hat{\mathcal{H}}_{\rm SOC} = -i\lambda \sum_{ij\sigma\sigma'} \hat{c}^\dagger_{i+\boldsymbol{d}_j\sigma}(\boldsymbol{d}_j \times \hat{\boldsymbol{\sigma}}^{\sigma\sigma'}) \cdot \hat{w}\, \hat{c}_{i\sigma'}, \tag{6}$$

where the vector $\boldsymbol{d}_j = (d_j^x, d_j^y, 0)$ corresponds to the nearest neighbors of the ith site (Fig. 2), and $\hat{\boldsymbol{\sigma}} = (\sigma_x, \sigma_y, \sigma_z)$ consists of the Pauli matrices. The unit vector $\hat{w}$ shows a direction of the spin-orbit field, which in general can be arbitrary, but we restrict our considerations to the in-plane $\hat{w} \equiv \hat{x} = (1,0,0)$ and out-of-plane $\hat{z} = (0,0,1)$ polarizations, so formally we have

$$(\boldsymbol{d}_j \times \hat{\boldsymbol{\sigma}}) \cdot \hat{w} = \begin{cases} d_j^y \sigma_z & \text{for in-plane field,} \\ d_j^x \sigma_y - d_j^y \sigma_x & \text{for out-of-plane field.} \end{cases} \tag{7}$$

Let us notice that the out-of-plane component mixes $\uparrow$ and $\downarrow$ particles, whereas the in-plane field corresponds to additional spin-conserving hopping with the spin- and direction-dependent amplitude.

Bogoliubov–de Gennes technique

Magnetic impurities break the translational invariance of the system, therefore the local pairing amplitude χ_i and occupancy $n_{i\sigma}$ have to be determined for each lattice site individually [45]. One can diagonalize the Hamiltonian (1) via the following unitary transformation:

$$\hat{c}_{i\sigma} = \sum_n (u_{in\sigma}\hat{\gamma}_n - \sigma v^*_{in\sigma}\hat{\gamma}^\dagger_n), \tag{8}$$

where $\hat{\gamma}_n$ and $\hat{\gamma}^\dagger_n$ are *quasi*particle fermionic operators, with the eigenvectors $u_{in\sigma}$ and $v_{in\sigma}$. This leads to the Bogoliubov–de Gennes (BdG) equations [46]

$$\mathcal{E}_n \begin{pmatrix} u_{in\uparrow} \\ v_{in\downarrow} \\ u_{in\downarrow} \\ v_{in\uparrow} \end{pmatrix} = \sum_j \begin{pmatrix} H_{ij\uparrow} & D_{ij} & S^{\uparrow\downarrow}_{ij} & 0 \\ D^*_{ij} & -H^*_{ij\downarrow} & 0 & S^{\downarrow\uparrow}_{ij} \\ S^{\downarrow\uparrow}_{ij} & 0 & H_{ij\downarrow} & D_{ij} \\ 0 & S^{\uparrow\downarrow}_{ij} & D^*_{ij} & -H^*_{ij\uparrow} \end{pmatrix} \begin{pmatrix} u_{jn\uparrow} \\ v_{jn\downarrow} \\ u_{jn\downarrow} \\ v_{jn\uparrow} \end{pmatrix} \tag{9}$$

containing the single-particle term $H_{ij\sigma} = -t\delta_{\langle i,j\rangle} - [\tilde{\mu}_{i\sigma} + (K - \sigma J)\delta_{i0}]\delta_{ij} + S^{\sigma\sigma}_{ij}$ and the spin-orbit coupling term $S^{\sigma\sigma'}_{ij} = -i\lambda \sum_l (\boldsymbol{d}_l \times \hat{\boldsymbol{\sigma}}^{\sigma\sigma'}) \cdot \hat{w}\, \delta_{j,i+\boldsymbol{d}_l}$. Here, $S^{\sigma\sigma}_{ij}$ and $S^{\sigma\bar{\sigma}}_{ij}$ correspond to the in-plane and out-of-plane spin-orbit field, respectively, which satisfy $S^{\sigma\sigma'}_{ij} = (S^{\sigma'\sigma}_{ji})^*$, and $D_{ij} = U\chi_i\delta_{ij}$ describes the on-site pairing. The superconducting order parameter χ_i and occupancy $n_{i\sigma}$ can be computed self-consistently from the BdG equations (9),

$$\chi_i = \sum_n [u_{in\downarrow}v^*_{in\uparrow} f(\mathcal{E}_n) - u_{in\uparrow}v^*_{in\downarrow} f(-\mathcal{E}_n)], \tag{10}$$

$$n_{i\sigma} = \sum_n [|u_{in\sigma}|^2 f(\mathcal{E}_n) + |v_{in\bar{\sigma}}|^2 f(-\mathcal{E}_n)], \tag{11}$$

where $f(\omega) = 1/[1 + \exp(\omega/k_BT)]$ is the Fermi-Dirac distribution. In particular, the spin-resolved local density of states

(LDOS) is given by [47]

$$\rho_{i\sigma}(\omega) = \sum_n [|u_{in\sigma}|^2 \delta(\omega - \mathcal{E}_n) + |v_{in\sigma}|^2 \delta(\omega + \mathcal{E}_n)]. \quad (12)$$

For its numerical determination, we have replaced the Dirac δ function by the Lorentzian $\delta(\omega) = \zeta/[\pi(\omega^2 + \zeta^2)]$ with a small broadening $\zeta = 0.025t$.

III. NUMERICAL RESULTS AND DISCUSSION

We now present the BdG results obtained for the single impurity embedded in a triangular lattice (Sec. III A) and for several configurations of two magnetic impurities (Sec. III B). Numerical computations have been done at zero temperature for the finite cluster $N_a \times N_b = 41 \times 41$, assuming $U/t = -3$, $\mu/t = 0$, $K/t = 0$, and determining the bound states for varying J. In this work, we focus on the effect of an in-plane spin-orbit field, and additional results for the out-of-plane SOC are shown in the Supplemental Material (SM) [48].

A. Single magnetic impurity

Let us start by discussing the results obtained in the absence of spin-orbit coupling. A typical quasiparticle spectrum is displayed in Fig. 3, where we can recognize the gapped region $|\omega| \leqslant \Delta$ of the superconducting host (for our set of model parameters $\Delta \simeq 0.65t$) and one pair of the bound states, appearing symmetrically around the chemical potential. The energies $\pm E_\alpha$ of these states and spectral weights depend on the coupling J. In particular, at some critical J_c (indicated by black arrows) they eventually cross each other. This crossing is a hallmark of the quantum phase transition (QPT) [49] in which the ground state undergoes a qualitative evolution [15]. When magnetic coupling overcomes the pairing energy (for $|J| \geqslant J_c$), the particle and hole states become degenerate, and the ground state changes from a BCS singlet to a spinful configuration [15,50–52].

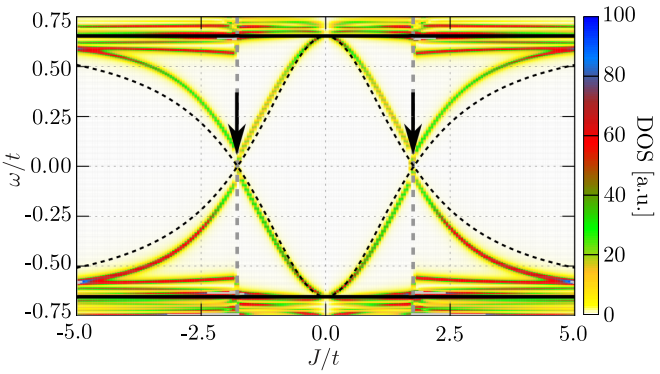

FIG. 3. Evolution of the low-energy spectrum with respect to the magnetic coupling J. The solid black line shows the magnitude of the pairing gap in regions far away from the impurity, black arrows point to the quantum phase transition (i.e., crossing of the subgap YSR states), and thin-dashed lines display the YSR bound states calculated from Eq. (13). Results were obtained without the SOC.

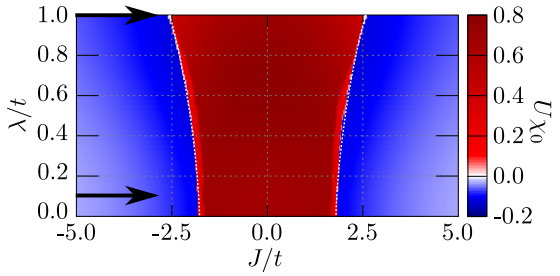

FIG. 4. Influence of the in-plane SOC on the critical value J_c. Blue and red correspond to the discontinuous change of $U\chi_0$ at the impurity site, and a white line marks the QPT. Black arrows indicate two values of λ, for which the profiles are shown in Fig. 5.

Our BdG data can be confronted with the analytical results of the thermodynamic limit $N_a \times N_b \to \infty$ [50]:

$$E_{\mathrm{YSR}} = \pm\Delta \frac{1-\alpha^2}{1+\alpha^2}, \quad (13)$$

where $\alpha = \pi\rho_0 J$ is the dimensionless impurity coupling parameter, ρ_0 is the normal state DOS at the Fermi level, and Δ is the superconducting gap. These quasiparticle energies (13) are displayed in Fig. 3 by a thin-dashed line. In the weak-coupling limit $|J| \leqslant J_c$, the formula (13) matches well with our numerical BdG results. Some differences appear above the QPT (for $|J| \geqslant J_c$), where the local pairing parameter at magnetic impurity is substantially reduced, affecting also the pairing gap of its neighboring sites. With an increasing coupling λ, the QPT is shifted to higher values (Fig. 4). The critical J_c corresponds to a value of J at which the YSR states cross each other. Variation of the critical J_c is caused by the influence of the SOC merely on the normal state DOS (ρ_0).

Such a quantum phase transition is manifested by a sign change of the order parameter χ_0 at the impurity site [Fig. 5(a)],

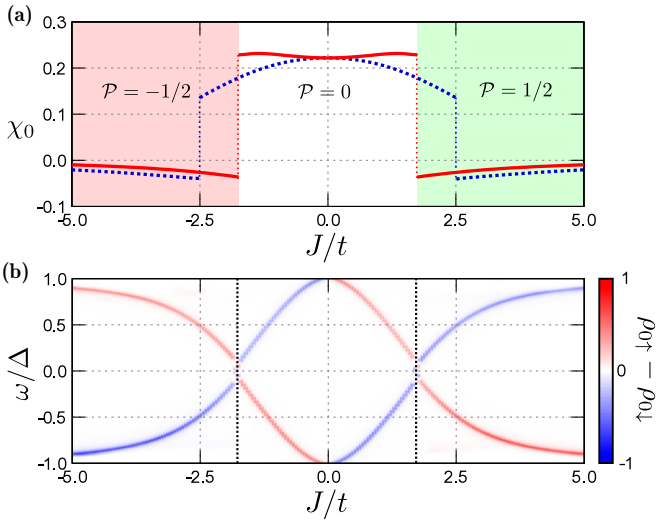

FIG. 5. The order parameter $\chi_0 = \langle \hat{c}_{0\downarrow}\hat{c}_{0\uparrow}\rangle$ obtained at the impurity site $i = 0$ (a) for the weak (red line) and strong (blue dotted line) spin-orbit couplings, with $\lambda/t = 0.1$ and 1.0, respectively. Magnetic polarization of the YSR states $\rho_{0\uparrow}(\omega) - \rho_{0\downarrow}(\omega)$ (b), obtained for $\lambda/t = 0.1$.

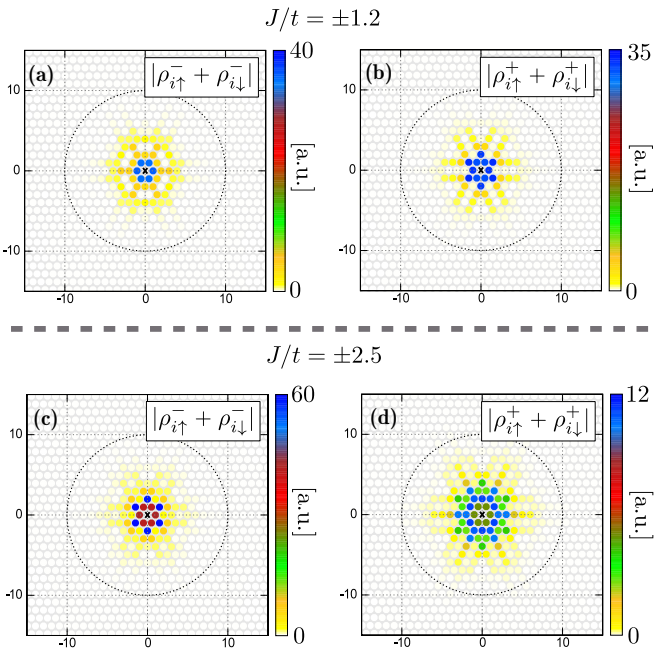

FIG. 6. Spatial patterns of the "negative" and "positive" YSR states $|\bar{\rho}^{\pm}_{i\uparrow} + \bar{\rho}^{\pm}_{i\downarrow}|$. Results are obtained for $J/t = \pm 1.2$ (top panel) and $J/t = \pm 2.5$ (bottom panel), assuming the in-plane spin-orbit coupling $\lambda/t = 0.1$.

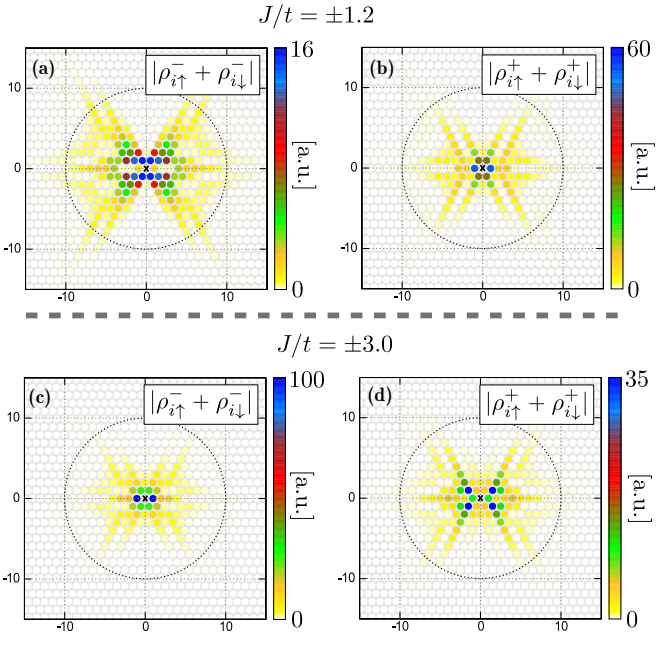

FIG. 7. The same as in Fig. 6, but for the stronger spin-orbit interaction $\lambda/t = 1$.

and discontinuity of its absolute value is a signature of the first-order phase transition [53–55]. Let us emphasize that the QPT is associated also with a reversal of the YSR polarization [Fig. 5(b)] and furthermore the total polarization of the system $\mathcal{P} = \frac{1}{2}\sum_i (n_{i\uparrow} - n_{i\downarrow})$ abruptly changes at $J = \pm J_c$ from zero to $\pm 1/2$ [56]. Similar behavior can be observed for multiple impurities [57].

In the weak-coupling limit (i.e., for $\lambda \ll t$), we can hardly notice any meaningful influence of SOC on the bulk superconductivity and the YSR states (see Fig. 1 in the SM [48]). A similar conclusion has been previously reported from the T-matrix treatment of magnetic impurities for 1D and 2D square lattices by Kaladzhyan *et al.* [52]. Our calculations have been done for $\lambda/t = 0.1$ which could be realistic for the $NbSe_2$ compound. Obviously for much stronger values of the spin-orbit coupling, both the superconducting state and the bound YSR states depend on the magnitude of λ and the direction of the magnetic moment [58].

Let us now explore the spatial extent of the YSR states. This can be achieved within the BdG approach by integrating the spectral weights

$$\rho^{\pm}_{i\sigma} = \int_{\omega_1}^{\omega_2} \rho_{i\sigma}(\omega) d\omega \tag{14}$$

in the interval $\omega \in (\omega_1, \omega_2)$ capturing every in-gap quasiparticle below or above the Fermi level [59]. Our numerical calculations have been done for the single impurity in the weak $J = -1.2t > -J_c$ and strong magnetic coupling limits $J = -2.5t < -J_c$, respectively. The results shown in Fig. 6 (notice different scales for each of these panels) reveal the characteristic six-leg star shape, whose extent spreads on several sites around the magnetic impurity. Spectral weights at the positive and negative energies are quite different, leading to a finite spin polarization of the YSR states (displayed in the bottom panel in Fig. 5).

Upon varying J, we observe that the star-shape (characterizing the C_6 symmetry of a triangular lattice) is rather robust. Such YSR state patterns could be probed by scanning tunneling microscopy, which nowadays has an atomic-scale resolution [8,12,60–62]. Let us emphasize that this six-leg star shape originates from a triangular lattice geometry and from the particular topology of the Fermi surface [63], in agreement with the experimental observations [11]. We have checked that the YSR states are only quantitatively (by a few percent) affected by the weak ($\lambda/t = 0.1$) in-plane spin-orbit coupling. For stronger SOC, the results are presented in Fig. 7. Comparison with Fig. 6 shows that for higher λ the YSR states gradually increase their extent, and the starlike shape seems to be weakly deformed with some elongation parallel to the x axis. Figure 7(a) presents an especially large range of bound states, extending well beyond ten lattice constants from the impurity site. As stated in the previous section, the in-plane spin-orbit field leads to the presence of the $S^{\sigma\sigma}_{ij}$ term in the single-particle part of the BdG equations, which directly affects the hopping amplitude. To observe the influence of this term on the spectral function, λ has to be of the order of t. We suspect that the large spatial extent of the YSR states reported in [11] was a consequence of the reduced dimensionality and/or the structure of the atomic lattice, and was not affected much by the in-plane spin-orbit field of $NbSe_2$. In general, however, materials with the stronger SOC couplings could reveal some increase in the spatial extent of subgap bound states.

For some quantitative analysis of the spatial profiles of YSR states, we define the *displaced moving average* (DMA) $\bar{\rho}^{\pm}(r)$ interpreted as an averaged spectral weight contained in a ring of radius r and its half-width δr. It depends only on

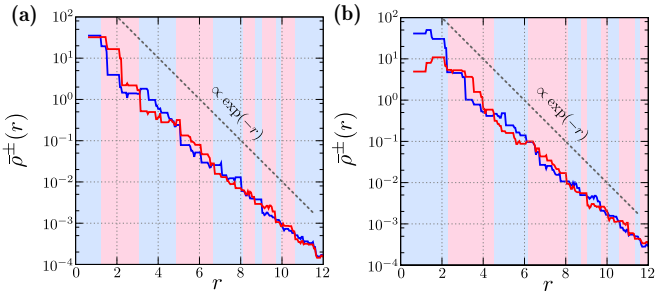

FIG. 8. Profiles of the hole- (blue line) and electron-like (red line) displaced moving average (DMA) for the YSR bound states $\bar{\rho}^{\pm}(r)$ as a function of distance r from the impurity (with $\delta r = 0.5$). The left and right panels correspond to $|J| < J_c$ and $|J| > J_c$, respectively. Results are obtained for the in-plane spin-orbit field $\lambda/t = 0.1$. The dashed gray line corresponds to $\exp(-r)$, which is a guide to eye. The blue (red) background indicates the dominant hole (particle) type of the YSR state at a given r.

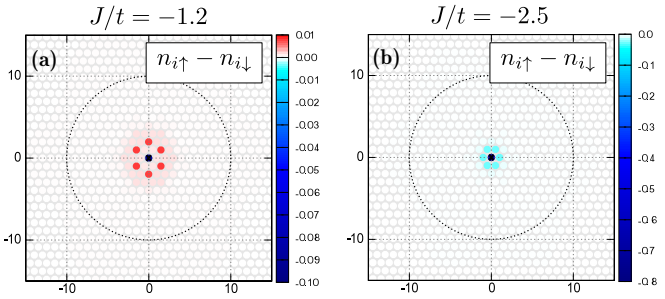

FIG. 9. Magnetization along the z axis induced near the magnetic impurity for $|J| < J_c$ (a) and $|J| > J_c$ (b).

a radial distance r from the magnetic impurity $\boldsymbol{r}_0$, averaging the angle-dependent fluctuations. Our results are presented in Fig. 8. They clearly show that functions $\bar{\rho}^{\pm}(r)$ of the YSR states are characterized by particle and hole oscillations that are opposite in phase (see the blue and red lines). Such particle-hole oscillations decay exponentially with distance (notice a logarithmic scale in Fig. 8), in agreement with previous studies [11,56,64]. In the 2D continuum version of this model, the wave functions of the YSR states have been expressed analytically [11]:

$$\psi^{\pm}(r) \propto \frac{1}{\sqrt{k_F r}} \sin\left(k_F r - \frac{\pi}{4} + \delta^{\pm}\right) \times \exp\left[-\sin(\delta^{+} - \delta^{-})\frac{r}{\zeta}\right], \quad (15)$$

where k_F is the Fermi wave vector, r is the distance from the impurity, whereas ζ is the superconducting coherence length. Both functions oscillate with $k_F r$, but with different scattering phase shifts $\delta^{\pm} = K\rho_0 \pm J/\rho_0$. At short distances, the YSR wave functions are governed by $\sin(k_F r)/\sqrt{k_F r}$, whereas for larger r the exponential envelope function suppresses particle-hole oscillations (see the dotted line in Fig. 8). Dominant (particle or hole) contributions to the YSR bound states are displayed by an alternating color of the background in Fig. 8. The period of such oscillations is approximately equal to nearly two lattice constants. The out-of-plane spin-orbit field leads to a similar behavior (Fig. 5 in [48]).

The quantum phase transition (at J_c) has consequences on a reversal of the magnetization induced near the impurity (see Fig. 9). For $|J| < J_c$, the impurity is weakly screened, whereas for stronger couplings, $|J| > J_c$, the impurity polarizes its neighborhood in the direction of its own magnetic moment. In both cases, this short-range magnetization does not coincide with the six-leg star shape of the bound states. Differences between the YSR wave functions and various components of magnetization have been previously discussed for a 2D square lattice by Kaladzhyan *et al.* [52].

B. YSR of double impurities

The BdG technique has the advantage that it can be easily applied to study the bound states of more numerous impurities, distributed at arbitrary positions in a crystallographic lattice. In this section, we consider the case of double magnetic impurities arranged in three different configurations displayed in Fig. 10(a). Our study of the YSR states is inspired by the results of Ref. [20] for ferromagnetic dimers. Such BdG calculations can be applied to more complex molecules [51,65–67] and/or multi-impurity structures [68–70]. It is well known [1] that multiple impurities can develop several quantum phase transitions with some characteristic features. They have been previously studied for 2D lattices, treating the spins classically [57,71,72] and taking into account the strong correlation effects within the Anderson-type scenario [73]. Here we explore the YSR states of two classical magnetic impurities embedded in a triangular lattice, assuming the weak in-plane spin orbit interaction $\lambda/t = 0.1$.

Figure 10 presents the subgap spectrum obtained for different configurations of the double impurities. We notice that coupling between the impurities induces the double-peak structure of YSR states, both at negative and positive energies [panel (b)]. Figure 11 displays spatial distributions of the YSR states for each configuration of the double magnetic impurities for the weak (left column) and strong (right column) couplings J. Although the C_6 rotational symmetry is broken, one can clearly see the mirror symmetry with respect to the axis

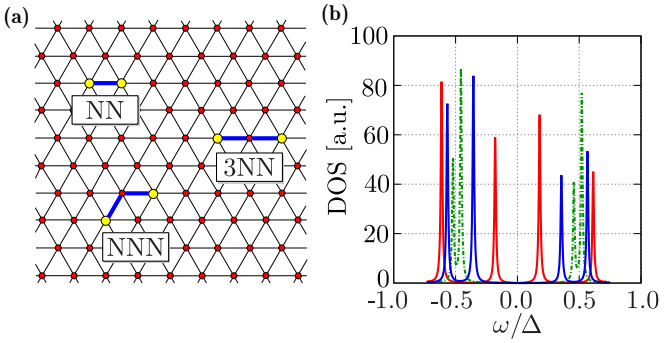

FIG. 10. Schematic illustration of two magnetic impurities arranged in three different configurations (a) and the subgap spectrum (b) for the nearest neighbors (NN), next nearest neighbors (NNN), and third nearest neighbors (3NN), as shown by red, blue, and green lines, respectively. We assumed the in-plane spin-orbit coupling $\lambda/t = 0.1$.

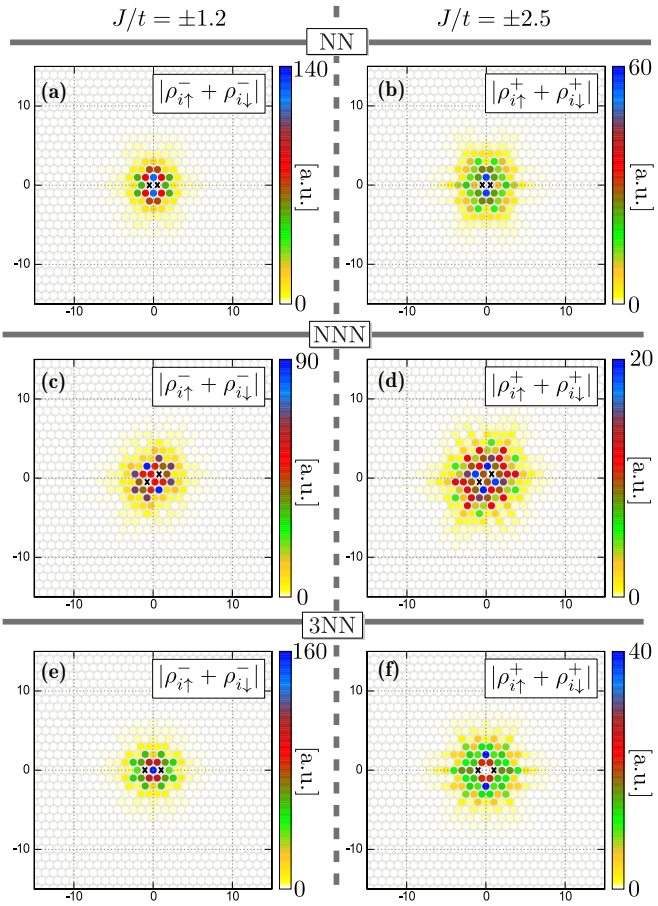

FIG. 11. Spatial pattern of the YSR states for the double magnetic impurities in different (NN, NNN, 3NN) configurations, as indicated. The left column panels refer to the weak coupling $J/t = -1.2$ and the right column panels to the strong coupling $J/t = -2.5$ limits, respectively. We imposed the in-plane spin-orbit coupling $\lambda/t = 0.1$ that could be relevant to $NbSe_2$.

connecting these double impurities and the axis perpendicular to it. Novel spatial patterns of the YSR states are due to the constructive/destructive quantum interference between the overlapping subgap states. Obviously, the most significant quantum interference occurs for the quantum impurities either at the nearest-neighbor (NN) or next-nearest-neighbor (NNN) configurations, with a clear bonding-antibonding splitting of the YSR quasiparticle energies. For more distant arrangements of the double impurities (for instance, 3NN), their spatial patterns gradually evolve back to the starlike shape. A more in-depth comparison of the results obtained with and without SOC is presented in [48] Figs. 6 and 7 of the SM. We hope that our theoretical predictions can be empirically verified, using the combined AFM (capable of manipulating the impurities) and STM (suitable for probing the subgap spectrum) techniques.

IV. CONCLUSIONS

In summary, we have investigated the energies and spatial extent of the Yu-Shiba-Rusinov (YSR) states induced by the classical magnetic impurities embedded in a two-dimensional triangular lattice of the 2H-$NbSe_2$ superconducting host. To study this particular crystallographic geometry in the presence of local inhomogeneities (in a form of the single or double impurities) and the spin-orbit coupling (SOC), we have adopted the Bogoliubov–de Gennes formalism.

In agreement with experimental observations [11], we have found that the YSR states acquire sixfold rotational symmetry (starlike patterns) whose spectroscopic signatures extend onto about a dozen of the intersite distances. Furthermore, their intertwining (π-shifted in phase) particle-hole oscillations are clearly visible. The weak spin-orbit coupling (which should be relevant to the 2H-$NbSe_2$ compound) has a rather negligible influence on the energies of YSR states, but for relatively stronger SOC their spatial extent eventually increases (beyond 10 lattice constants in some cases). Analysis of the SOC for the single impurity indicates that the extended range of YSR states reported in [11] stems from the dimensionality and/or the structure of an atomic lattice, rather than from the in-plane spin-orbit field of such materials.

We have also studied the subgap quasiparticle spectrum of double magnetic impurities in three different configurations, revealing either the constructive or destructive quantum interference that breaks C_6 symmetry of the YSR wave functions. Deviation from the starlike shape (typical for single impurities) depends on the relative distance between such magnetic impurities. When they are close to each other, the YSR states develop a double-peak structure (characteristic for the bonding and antibonding states) whose spatial patterns no longer resemble the star shape. With an increasing distance between the impurities, such bonding-antibonding splitting gradually disappears, and the spatial starlike shape of YSR states is gradually restored.

ACKNOWLEDGMENTS

We thank K. J. Kapcia for valuable comments and discussions. This work was supported by the National Science Centre (NCN, Poland) under Grants No. UMO-2016/20/S/ST3/00274 (A.P.) and No. DEC-2014/13/B/ST3/04451 (S.G. and T.D.)

[1] A. V. Balatsky, I. Vekhter, and J.-X. Zhu, Impurity-induced states in conventional and unconventional superconductors, Rev. Mod. Phys. **78**, 373 (2006).

[2] V. Koerting, B. M. Andersen, K. Flensberg, and J. Paaske, Nonequilibrium transport via spin-induced subgap states in superconductor/quantum dot/normal metal cotunnel junctions, Phys. Rev. B **82**, 245108 (2010).

[3] B. W. Heinrich, J. I. Pascual, and K. J. Franke, Single magnetic adsorbates on s-wave superconductors, arXiv:1705.03672.

[4] L. Yu, Bound state in superconductors with paramagnetic impurities, Acta Phys. Sin. **21**, 75 (1965).

[5] H. Shiba, Classical spins in superconductors, Prog. Theor. Exp. Phys. **40**, 435 (1968).

[6] A. I. Rusinov, Superconductivity near a paramagnetic impurity, Zh. Eksp. Teor. Fiz. Pisma Red. **9**, 146 (1968) [JETP Lett. **9**, 85 (1969)].

[7] A. Yazdani, B. A. Jones, C. P. Lutz, M. F. Crommie, and D. M. Eigler, Probing the local effects of magnetic impurities on superconductivity, Science **275**, 1767 (1997).

[8] S.-H. Ji, T. Zhang, Y.-S. Fu, X. Chen, X.-C. Ma, J. Li, W.-H. Duan, J-F. Jia, and Q.-K. Xue, High-Resolution Scanning Tunneling Spectroscopy of Magnetic Impurity Induced Bound States in the Superconducting Gap of Pb Thin Films, Phys. Rev. Lett. **100**, 226801 (2008).

[9] M. Ruby, F. Pientka, Y. Peng, F. von Oppen, B. W. Heinrich, and K. J. Franke, Tunneling Processes into Localized Subgap States in Superconductors, Phys. Rev. Lett. **115**, 087001 (2015).

[10] N. Hatter, B. W. Heinrich, M. Ruby, J. I. Pascual, and K. J. Franke, Magnetic anisotropy in Shiba bound states across a quantum phase transition, Nat. Commun. **6**, 8988 (2015).

[11] G. C. Ménard, S. Guissart, C. Brun, S. Pons, V. S. Stolyarov, F. Debontridder, M. V. Leclerc, E. Janod, L. Cario, D. Roditchev, P. Simon, and T. Cren, Coherent long-range magnetic bound states in a superconductor, Nat. Phys. **11**, 1013 (2015).

[12] D.-J. Choi, C. Rubio-Verdú, J. de Bruijckere, M. M. Ugeda, N. Lorente, and J. I. Pascual, Mapping the orbital structure of impurity bound states in a superconductor, Nat. Commun. **8**, 15175 (2017).

[13] A. Assouline, Ch. Feuillet-Palma, A. Zimmers, H. Aubin, M. Aprili, and J.-Ch. Harmand, Shiba Bound States Across the Mobility Edge in Doped InAs Nanowires, Phys. Rev. Lett. **119**, 097701 (2017).

[14] A. Jellinggaard, K. Grove-Rasmussen, M. H. Madsen, and J. Nygård, Tuning Yu-Shiba-Rusinov states in a quantum dot, Phys. Rev. B **94**, 064520 (2016).

[15] M. I. Salkola, A. V. Balatsky, and J. R. Schrieffer, Spectral properties of quasiparticle excitations induced by magnetic moments in superconductors, Phys. Rev. B **55**, 12648 (1997).

[16] M. E. Flatté and J. M. Byers, Local Electronic Structure of a Single Magnetic Impurity in a Superconductor, Phys. Rev. Lett. **78**, 3761 (1997).

[17] A. L. Fetter, Spherical impurity in an infinite superconductor, Phys. Rev. **140**, A1921 (1965).

[18] M. M. Ugeda, A. J. Bradley, Y. Zhang, S. Onishi, Y. Chen, W. Ruan, C. Ojeda-Aristizabal, H. Ryu, M. T. Edmonds, H.-Z. Tsai, A. Riss, S.-K. Mo, D. Lee, A. Zettl, Z. Hussain, Z.-X. Shen, and M. F. Crommie, Characterization of collective ground states in single-layer $NbSe_2$, Nat. Phys. **12**, 92 (2016).

[19] X. Xi, Z. Wang, W. Zhao, J.-H. Park, K. T. Law, H. Berger, L. Forro, J. Shan, and K. F. Mak, Ising pairing in superconducting $NbSe_2$ atomic layers, Nat. Phys. **12**, 139 (2016).

[20] S. Kezilebieke, M. Dvorak, T. Ojanen, and P. Liljeroth, Coupled Yu-Shiba-Rusinov states in molecular dimers on $NbSe_2$, arXiv:1701.03288.

[21] L. Bawden, S. P. Cooil, F. Mazzola, J. M. Riley, L. J. Collins-McIntyre, V. Sunko, K. W. B. Hunvik, M. Leandersson, C. M. Polley, T. Balasubramanian, T. K. Kim, M. Hoesch, J. W. Wells, G. Balakrishnan, M. S. Bahramy, and P. D. C. King, Spin-valley locking in the normal state of a transition-metal dichalcogenide superconductor, Nat. Commun. **7**, 11711 (2016).

[22] A. Meerschaut and C. Deudon, Crystal structure studies of the 3R-$Nb_{1.09}S_2$ and the 2H-$NbSe_2$ compounds: Correlation between nonstoichiometry and stacking type (= polytypism), Mater. Res. Bull. **36**, 1721 (2001).

[23] J. M. Riley, F. Mazzola, M. Dendzik, M. Michiardi, T. Takayama, L. Bawden, C. Granerød, M. Leandersson, T. Balasubramanian, M. Hoesch, T. K. Kim, H. Takagi, W. Meevasana, Ph. Hofmann, M. S. Bahramy, J. W. Wells, and P. D. C. King, Direct observation of spin-polarised bulk bands in an inversion-symmetric semiconductor, Nat. Phys. **10**, 835 (2014).

[24] X. Zhang, Q. Liu, J.-W. Luo, A. J. Freeman, and A. Zunger, Hidden spin polarization in inversion-symmetric bulk crystals, Nat. Phys. **10**, 387 (2014).

[25] J. M. Riley, W. Meevasana, L. Bawden, M. Asakawa, T. Takayama, T. Eknapakul, T. K. Kim, M. Hoesch, S. K. Mo, H. Takagi, T. Sasagawa, M. S. Bahramy, and P. D. C. King, Negative electronic compressibility and tunable spin splitting in WSe_2, Nat. Nanotechnol. **10**, 1043 (2015).

[26] J. A. Wilson, F. J. Di Salvo, and S. Mahajan, Charge-Density Waves in Metallic, Layered, Transition-Metal Dichalcogenides, Phys. Rev. Lett. **32**, 882 (1974).

[27] X. Zhu, Y. Cao, J. Zhang, E. W. Plummer, and J. Guo, Classification of charge density waves based on their nature, Proc. Natl. Acad. Sci. (U.S.A.) **112**, 2367 (2015).

[28] T. Yokoya, T. Kiss, A. Chainani, S. Shin, M. Nohara, and H. Takagi, Fermi surface sheet-dependent superconductivity in $2H$-$NbSe_2$, Science **294**, 2518 (2001).

[29] S. V. Borisenko, A. A. Kordyuk, V. B. Zabolotnyy, D. S. Inosov, D. Evtushinsky, B. Büchner, A. N. Yaresko, A. Varykhalov, R. Follath, W. Eberhardt, L. Patthey, and H. Berger, Two Energy Gaps and Fermi-Surface "Arcs" in $NbSe_2$, Phys. Rev. Lett. **102**, 166402 (2009).

[30] D. J. Rahn, S. Hellmann, M. Kalläne, C. Sohrt, T. K. Kim, L. Kipp, and K. Rossnagel, Gaps and kinks in the electronic structure of the superconductor $2H$-$NbSe_2$ from angle-resolved photoemission at 1 K, Phys. Rev. B **85**, 224532 (2012).

[31] K. Rossnagel, O. Seifarth, L. Kipp, M. Skibowski, D. Voß, P. Krüger, A. Mazur, and J. Pollmann, Fermi surface of $2H$-$NbSe_2$ and its implications on the charge-density-wave mechanism, Phys. Rev. B **64**, 235119 (2001).

[32] M. D. Johannes, I. I. Mazin, and C. A. Howells, Fermi-surface nesting and the origin of the charge-density wave in $NbSe_2$, Phys. Rev. B **73**, 205102 (2006).

[33] F. Flicker and J. van Wezel, Charge order from orbital-dependent coupling evidenced by $NbSe_2$, Nat. Commun. **6**, 7034 (2015).

[34] J. Á. Silva-Guillén, P. Ordejón, F. Guinea, and E. Canadell, Electronic structure of $2H$-$NbSe_2$ single-layers in the CDW state, 2D Mater. **3**, 035028 (2016).

[35] K. Momma and F. Izumi, *VESTA3* for three-dimensional visualization of crystal, volumetric and morphology data, J. Appl. Crystallogr. **44**, 1272 (2011).

[36] H. Zeng, J. Dai, W. Yao, D. Xiao, and X. Cui, Valley polarization in MoS_2 monolayers by optical pumping, Nat. Nanotech. **7**, 490 (2012).

[37] K. F. Mak, K. He, J. Shan, and T. F. Heinz, Control of valley polarization in monolayer MoS_2 by optical helicity, Nat. Nanotech. **7**, 494 (2012).

[38] R. Suzuki, M. Sakano, Y. J. Zhang, R. Akashi, D. Morikawa, A. Harasawa, K. Yaji, K. Kuroda, K. Miyamoto, T. Okuda, K. Ishizaka, R. Arita, and Y. Iwasa, Valley-dependent spin polarization in bulk MoS_2 with broken inversion symmetry, Nat. Nanotech. **9**, 611 (2014).

[39] B. Zhu, H. Zeng, J. Dai, Z. Gong, and X. Cui, Anomalously robust valley polarization and valley coherence in bilayer WS_2, Proc. Natl. Acad. Sci. (U.S.A.) **111**, 11606 (2014).

[40] S. Glass, G. Li, F. Adler, J. Aulbach, A. Fleszar, R. Thomale, W. Hanke, R. Claessen, and J. Schäfer, Triangular Spin-Orbit-Coupled Lattice with Strong Coulomb Correlations: Sn Atoms on a SiC(0001) Substrate, Phys. Rev. Lett. **114**, 247602 (2015).

[41] G. Sharma and S. Tewari, Yu-Shiba-Rusinov states and topological superconductivity in Ising paired superconductors, Phys. Rev. B **94**, 094515 (2016).

[42] E. D. B. Smith, K. Tanaka, and Y. Nagai, Manifestation of chirality in the vortex lattice in a two-dimensional topological superconductor, Phys. Rev. B **94**, 064515 (2016).

[43] S. L. Goertzen, K. Tanaka, and Y. Nagai, Self-consistent study of Abelian and non-Abelian order in a two-dimensional topological superconductor, Phys. Rev. B **95**, 064509 (2017).

[44] Y. Xu, Ch. Qu, M. Gong, and Ch. Zhang, Competing superfluid orders in spin-orbit-coupled fermionic cold-atom optical lattices, Phys. Rev. A **89**, 013607 (2014).

[45] A. Ptok and K. J. Kapcia, Probe-type of superconductivity by impurity in materials with short coherence length: The s-wave and η-wave phases study, Supercond. Sci. Technol. **28**, 045022 (2015).

[46] P. G. De Gennes, *Superconductivity of Metals and Alloys*, Advanced Books Classics Series (Westview, 1999).

[47] H. Matsui, T. Sato, T. Takahashi, S.-C. Wang, H.-B. Yang, H. Ding, T. Fujii, T. Watanabe, and A. Matsuda, BCS-Like Bogoliubov Quasiparticles in High-T_c Superconductors Observed by Angle-Resolved Photoemission Spectroscopy, Phys. Rev. Lett. **90**, 217002 (2003).

[48] See Supplemental Material at http://link.aps.org/supplemental/10.1103/PhysRevB.96.184425 for a comparison with results for out-of-plane spin-orbit coupling.

[49] A. Sakurai, Comments on superconductors with magnetic impurities, Prog. Theor. Phys. **44**, 1472 (1970).

[50] W. V. van Gerven Oei, D. Tanasković, and R. Žitko, Magnetic impurities in spin-split superconductors, Phys. Rev. B **95**, 085115 (2017).

[51] K. J. Franke, G. Schulze, and J. I. Pascual, Competition of superconducting phenomena and Kondo screening at the nanoscale, Science **332**, 940 (2011).

[52] V. Kaladzhyan, C. Bena, and P. Simon, Characterizing p-wave superconductivity using the spin structure of Shiba states, Phys. Rev. B **93**, 214514 (2016).

[53] M. Mashkoori, K. Björnson, and A. M. Black-Schaffer, Impurity bound states in fully gapped d-wave superconductors with subdominant order parameters, Sci. Rep. **7**, 44107 (2017).

[54] S. S. Pershoguba, K. Björnson, A. M. Black-Schaffer, and A. V. Balatsky, Currents Induced by Magnetic Impurities in Superconductors with Spin-Orbit Coupling, Phys. Rev. Lett. **115**, 116602 (2015).

[55] Sz. Głodzik and A. Ptok, Quantum phase transition induced by magnetic impurity, J. Supercond. Nov. Magn. (2017).

[56] D. K. Morr and N. A. Stavropoulos, Quantum interference between impurities: Creating novel many-body states in s-wave superconductors, Phys. Rev. B **67**, 020502 (2003).

[57] D. K. Morr and J. Yoon, Impurities, quantum interference, and quantum phase transitions in s-wave superconductors, Phys. Rev. B **73**, 224511 (2006).

[58] Y. Kim, J. Zhang, E. Rossi, and R. M. Lutchyn, Impurity-Induced Bound States in Superconductors with Spin-Orbit Coupling, Phys. Rev. Lett. **114**, 236804 (2015).

[59] J. Röntynen and T. Ojanen, Topological Superconductivity and High Chern Numbers in 2D Ferromagnetic Shiba Lattices, Phys. Rev. Lett. **114**, 236803 (2015).

[60] M. T. Randeria, B. E. Feldman, I. K. Drozdov, and A. Yazdani, Scanning Josephson spectroscopy on the atomic scale, Phys. Rev. B **93**, 161115 (2016).

[61] H. Kim, Y. Yoshida, Ch.-Ch. Lee, T.-R. Chang, H.-T. Jeng, H. Lin, Y. Haga, Z. Fisk, and Y. Hasegawa, Atomic-scale visualization of surface-assisted orbital order, arXiv:1706.09753.

[62] G. Reecht, B. Heinrich, H. Bulou, F. Scheurer, L. Limot, and G. Schull, Imaging isodensity contours of molecular states with STM, arXiv:1703.05622.

[63] A. Weismann, M. Wenderoth, P. Lounis, S. Zahn, N. Quaas, R. G. Ulbrich, P. H. Dederichs, and S. Blügel, Seeing the Fermi surface in real space by nanoscale electron focusing, Science **323**, 1190 (2009).

[64] T. Kawakami and X. Hu, Evolution of Density of States and a Spin-Resolved Checkerboard-Type Pattern Associated with the Majorana Bound State, Phys. Rev. Lett. **115**, 177001 (2015).

[65] D. Jacob, M. Soriano, and J. J. Palacios, Kondo effect and spin quenching in high-spin molecules on metal substrates, Phys. Rev. B **88**, 134417 (2013).

[66] J. Kügel, M. Karolak, A. Krönlein, J. Senkpiel, P.-J. Hsu, G. Sangiovanni, and M. Bode, State identification and tunable Kondo effect of MnPc on Ag(001), Phys. Rev. B **91**, 235130 (2015).

[67] J. O. Island, R. Gaudenzi, J. de Bruijckere, E. Burzurí, C. Franco, M. Mas-Torrent, C. Rovira, J. Veciana, T. M. Klapwijk, R. Aguado, and H. S. J. van der Zant, Proximity-Induced Shiba States in a Molecular Junction, Phys. Rev. Lett. **118**, 117001 (2017).

[68] S. Nakosai, Y. Tanaka, and N. Nagaosa, Two-dimensional p-wave superconducting states with magnetic moments on a conventional s-wave superconductor, Phys. Rev. B **88**, 180503 (2013).

[69] G. C. Ménard, S. Guissart, Ch. Brun, M. Trif, F. Debontridder, R. T. Leriche, D. Demaille, D. Roditchev, P. Simon, and T. Cren, Two-dimensional topological superconductivity in Pb/Co/Si(111), arXiv:1607.06353.

[70] J. L. Lado and J. Fernández-Rossier, Unconventional Yu-Shiba-Rusinov states in hydrogenated graphene, 2D Mater. **3**, 025001 (2016).

[71] S. Hoffman, J. Klinovaja, T. Meng, and D. Loss, Impurity-induced quantum phase transitions and magnetic order in conventional superconductors: Competition between bound and quasiparticle states, Phys. Rev. B **92**, 125422 (2015).

[72] T. Meng, J. Klinovaja, S. Hoffman, P. Simon, and D. Loss, Superconducting gap renormalization around two magnetic impurities: From Shiba to Andreev bound states, Phys. Rev. B **92**, 064503 (2015).

[73] R. Žitko, Numerical subgap spectroscopy of double quantum dots coupled to superconductors, Phys. Rev. B **91**, 165116 (2015).